J Solid State Electrochem (2012) 16:2103–2112
DOI 10.1007/s10008-011-1625-z

ORIGINAL PAPER

Effect of styrene–acrylonitrile content on 0.5 M NaI/0.05 M I_2 liquid electrolyte encapsulation for dye-sensitized solar cells

Wee Ching Tan · Siti Salwa Alias · Ahmad Badri Ismail · Ahmad Azmin Mohamad

Received: 29 July 2011 / Revised: 11 December 2011 / Accepted: 15 December 2011 / Published online: 29 December 2011

Abstract The effect of a gel polymer electrolyte (GPE) as the redox electrolyte used in dye-sensitized solar cells was studied. A GPE solution consisting of 0.5 M sodium iodide, 0.05 M iodine, and ethylene carbonate/propylene carbonate (1:1 *w*/*w*) binary solvents was mixed with increasing amounts of styrene–acrylonitrile (SAN). Bulk conductivity measurements show a decreasing trend from 4.54 to 0.83×10^{-3} S cm^{-1} with increasing SAN content. The GPE exhibits Newtonian-like behavior and its viscosity increases from 0.041 to 1.093 Pa s with increasing SAN content. A balance between conductivity (1.3×10^{-3} S cm^{-1}) and viscosity (1.4 Pa s) is observed at 19 wt.% SAN. Fourier transform infrared spectroscopy detects elevated ring torsion at 706 cm^{-1} upon the addition of SAN into the liquid electrolyte. This indicates that SAN does not bond with the liquid electrolyte. Finally, the potential stability window of 19 wt.% SAN, which ranges from −1.68 to 1.38 V, proves its applicability in solar cells.

Keywords Styrene–acrylonitrile · Conductivity · Viscosity · Fourier transform infrared spectroscopy · Linear sweep voltammetry

Introduction

Gel polymer electrolytes (GPE) used in solid and quasi-solid type charge transport materials have the advantages of high ionic conductivities, good contacts, and electrode-filling properties. GPEs are able to encapsulate liquid electrolytes thus, prevent problems such as leakage, evaporation of solvents, high temperature instability, flammability, and possible desorption [1]. Ramani et al. [2] claimed that copolymers of styrene have leverage in hydrolytic stability, and the introduction of a dopant can modify charge storage. This improves charge carrier mobility. The presence of an acrylonitrile monomer enhances the chemical resistance, rigidity, and strength of GPEs. Since most GPEs are amorphous in nature, Ileperuma et al. [3] suggested that acrylonitrile-based electrolytes can transport carriers by mediating through a segmental motion of the host polymer.

The styrene-acrylonitrile (SAN) copolymer exhibits some of the characteristics of each of its monomers. SAN has been used polymer composite production to enhance chemical stability and surface hardness while reducing weight [4]. It is also incorporated into proton conductive membranes to reduce costs while preserving the high conductivity and stability of polymer electrolyte membranes in fuel cells [5]. Pioneer works by Lan et al. [6] showed that SAN could be embedded into quasi-solid-state dye-sensitized solar cells (QSSCs) with nanoporous titanium dioxide as the photoelectrode. However, they only reported the effects of variations in iodide salt content, and summarized the best concentrations of salt complexes (0.5 M sodium iodide, 0.05 M iodine) for a constant amount of SAN. This combination of iodide salts in a mixture of ethylene carbonate (EC) and propylene carbonate (PC) in an acrylonitrile-based electrolyte was able to achieve a high room temperature conductivity of ~10^{-3} S cm^{-1} with good mechanical properties for solar cell applications [7].

SAN networks are used to absorb iodide solutions. Thus, appropriate concentrations of the polymer are essential in gel complexes. This is our primary interest. The effect of polymeric composition was explained by Sekhon [8] based on changes

W. C. Tan · S. S. Alias · A. B. Ismail · A. A. Mohamad (✉)
School of Materials and Mineral Resources Engineering,
Universiti Sains Malaysia,
Nibong Tebal 14300, Penang, Malaysia
e-mail: azmin@eng.usm.my

in carrier concentration and viscosity. A study on compositional effects is required to understand the role of SAN in the electrolyte, to describe the conductivity behavior with iodide/triiodide [I^-/I_3^-] kinetics toward charge interaction and storage ability, and to optimize gelled properties for continuous solar harvesting in the QSSC. The iodide species was utilized as part of the I^-/I_3^- redox couple, as shown in Eqs. 1–3:

$$I^- + I_2 \rightleftarrows I_3^- \quad (1)$$

$$3I^- + 2\text{dye}^+ \rightarrow I_3^- + 2\text{dye (photoelectrode)} \quad (2)$$

$$I_3^- + 2e^- \rightleftarrows 3I^- \text{(counter electrode)}. \quad (3)$$

In the present work, a liquid electrolyte with constant concentrations of 0.5 M sodium iodide (NaI) and 0.05 M iodine (I_2) is mixed with increasing concentrations of SAN. The resulting electrolytes are studied based on their conductivity, viscosity, diffusion coefficient, electrical stability, and thermal stability. Fourier transfer infrared (FTIR) spectroscopy is employed to study the changes of the bonds with increasing SAN content. The effect of polymeric content is determined by ensuring that the number of ions in the electrolyte remained constant, and the diffusivity of both I^- and I_3^- ions is found. Liquid electrolyte containment in SAN and the transfer of charges are proposed and discussed. The effect of temperature on conductivity and potential stability is studied as well. Finally, the optimized electrolyte, as determined by the sample with the highest conductivity, is assembled into an ITO/SAN+NaI+I_2/N719+ZnO+Zn solar cell.

Experimental

Preparation of electrolyte

The materials used included SAN (M_w ~165,000, Sigma-Aldrich) as the polymeric host, NaI (Sigma-Aldrich) and I_2 (Merck) as the I^-/I_3^- source, and EC (Merck) and PC (Merck) as the solvents. Required amounts of 0.5 M NaI and 0.05 M I_2 were mixed into EC and PC, forming a liquid electrolyte. Binary solvents of EC and PC in a 1:1 (*w*/*w*) ratio were mixed accordingly [9]. Increasing amounts of SAN were added to the electrolyte based on a variety of polymeric weight percentages. The mixtures were stirred vigorously at 75–85 °C for approximately 4 h until all the SAN pellets dissolved. The GPEs were then cooled to room temperature prior to testing.

Characterization of electrolytes

The Fourier transform infrared (PerkinElmer®) analysis was conducted in the wavelength range of 4,000–550 cm^{-1} at a spectral resolution of 4 cm^{-1} to study the changes of polymer structure with increasing SAN content at a constant salt concentration. The electrolytes were dropped onto a single reflectance diamond attenuated total reflectance crystal prior to the measurements.

The frequency response analyzer module in Autolab PGSTAT 30 (Eco Chemie, B.V.) system was employed to measure the bulk resistance (R_b) of as-prepared electrolytes with respect to increasing SAN content. The study on the effect of thermal dependence was also carried out in temperatures ranging from room temperature to 100 °C at increments of 5 °C.

The gelled state, as determined by the rheological behavior of gel the electrolyte, was tested via a viscotester (Haake Viscotester VT550). As-prepared electrolytes were transferred slowly to the sampler cup to ensure that no air bubbles were formed during loading. Viscosity measurements started at a strain rate of 10 s^{-1} and ended at 600 s^{-1}.

The potential stability of the polymer gel electrolytes was determined using the general purpose electrochemical solution module in Autolab PGSTAT 30. Linear sweep voltammetry (LSV) was conducted at a fixed potential range from −2.0 to 2.0 V.

A ZnO photoanode was prepared via the Zn-air method [10, 11] and immersed in 0.03 μM bis(tetrabutylammonium)-*cis*-(dithiocyanato)-*N*,*N*′-bis(4-carboxylato 4′carboxylic acid-2,2′-bipyridine) ruthenium(II) dye (N719, Aldrich) solution for 24 h to ensure full absorption. N-719 with concentration of 0.03 μM was diluted into 100 ml of anhydrous ethanol C_2H_5OH earlier. The anode was then removed from the dye solution, rinsed with absolute ethanol, and dried in an oven at 100 °C for 10 min. An indium tin oxide (ITO) counter photoelectrode was coated with silver paint to enhance its conducting pathway. About 40 μL of the optimized SAN-based electrolyte was dropped between the photoanodes, and two binder clips were used to hold the sandwiched structures in place for photocurrent–photovoltage (*I*–*V*) measurements (Autolab Potentiostat PGSTAT 30). The assembled QSSC was tested in both dark and tungsten halogen lamp-illuminated conditions for both liquid and gelled SAN-based GPEs. The applicability of the SAN-based electrolyte was studied based on the assembly shown in Fig. 1.

Results and discussion

Fourier transform infrared characterization

FTIR studies were conducted to determine the effect of increasing polymeric contents based on the structures in the SAN-based electrolyte. Results are shown in Fig. 2. Dotted peaks show the baselines of 0.5 M NaI, 0.05 M I_2, and solvent for the QSSC liquid electrolyte. The plot of

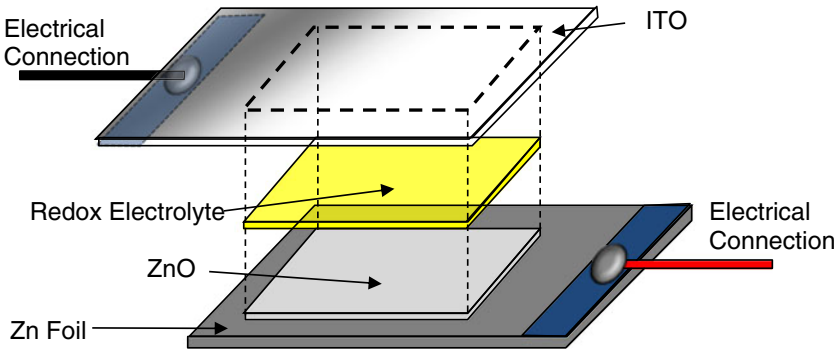

Fig. 1 Orientation of the QSSC system using a SAN-based electrolyte as a GPE

0 wt.% SAN served as the baseline for the "standard" redox electrolyte mixture. The peaks remained the same at 975, 1,055–1,073, 1,126, 1,359, 1,394, 1,431–1,461, 1,487, and 1,776–1,797 cm^{-1} regardless of SAN content. This indicates that no bonding occurs between SAN and the liquid electrolyte as shown in Fig. 2a.

However, a new peak was observed at 706 cm^{-1} upon the addition of 8 wt.% SAN (Fig. 2b). This suggests the occurrence of ring torsion, which was previously observed by Chowdhury and Thynell [12]. Table 1 shows the band assignments of the "standard" liquid redox electrolyte and the SAN-based quasi-solid electrolyte. The encapsulation of SAN in a liquid electrolyte is possible due to the formation of a charge transfer complex (CTC) between the phenyl group and I_2. Distortion of the phenyl group into a spatial agreement facilitates accommodation of the electrolytic components, ionic dissociation, and the diffusion of iodide species throughout the packed network. The new peak became more obvious with the introduction of more SAN, indicating the occurrence of more ring torsion in the phenyl group in the polymeric network.

The polymeric network in SAN consists of single bonds of C−C and C−C_6H_6. C−H bonds can rotate during mixture preparation under vigorous stirring and constant heat. The bonds along the main chain of SAN "soften" at a temperature high enough to provide sufficient thermal energy [13]. Thus, the bonds in SAN become more flexible and relatively softer (lower modulus), allowing redox liquid electrolytes to diffuse into the polymer network and be physically observed as a liquid-gel electrolyte.

Styrene-based polymers can be developed further into QSSCs with low packing density due to the existence of rigid spacers that keep the polymer chains apart [2]. Consequently, a space is created by phenyl distortion for electrolyte containment. This is shown by the occurrence of torsion in Fig. 2. SAN doped with I_2 allows sorption of NaI/I_2 liquid electrolyte by diffusion and when more and more segments of SAN molecules loosen, it forms the GPE. The affinity of

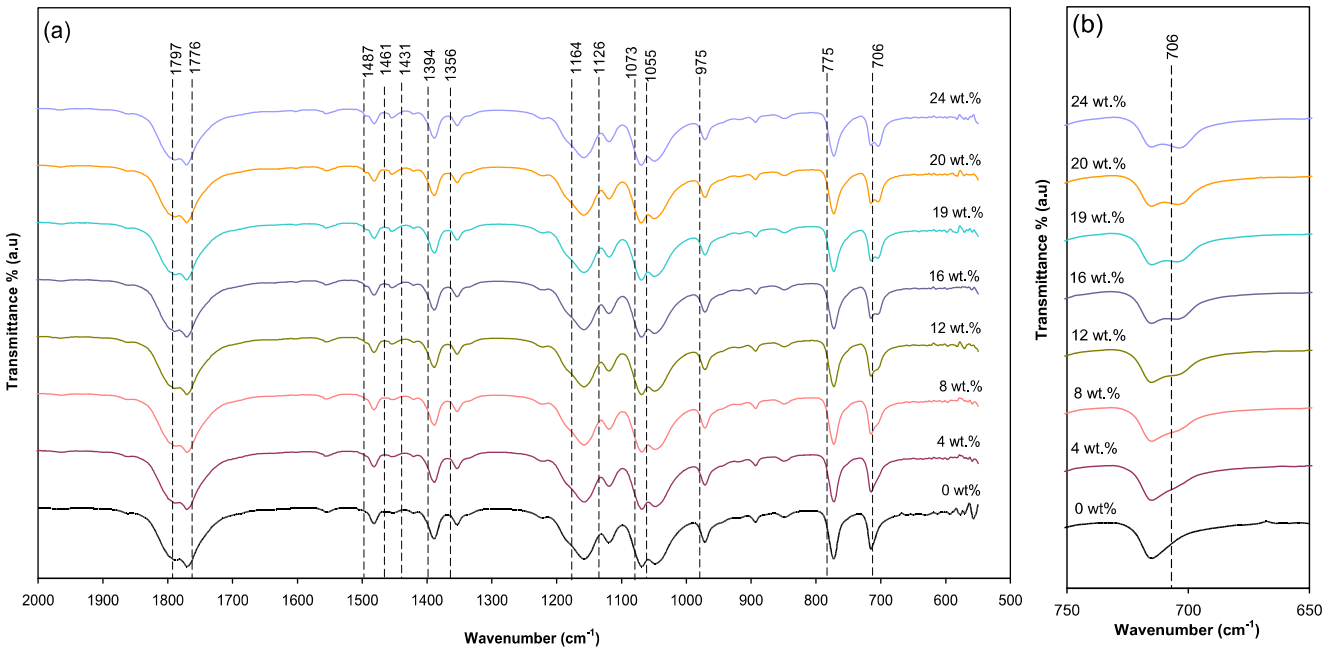

Fig. 2 FTIR spectra of GPEs with different SAN concentrations **a** in a range between 2,000 and 500 cm^{-1}; **b** at 706 cm^{-1}

Table 1 Band assignment of the "standard" liquid electrolyte with and without SAN

Description	Wave number (cm^{-1})	Reference
Ring torsion	706	[12]
PC and EC (out-of-plane CH bending)	975	[1]
PC (C–O symmetric stretching)	1,055–1,073	[34]
PC (ring twisting)	1,126	[34]
PC (ring, CH_3 symmetric stretching)	1,359	[34]
EC (CH_2 scissoring and wagging)	1,394	[35]
PC and EC (vibration of CH_2)	1,431–1,461	[36]
PC (CH_3 twisting)	1,487	[34]
PC and EC (C=O stretching)	1,776–1,797	[1]

I_2 toward the electrons in the phenyl group was studied utilizing the positron annihilation lifetime spectroscopy method [2]. Furthermore, Ramani et al. [2] proved that, among a range of different I_2 species tested, I_2 is able to encapsulate I_3^- species due to its free volume size in the SAN continuous phase.

A study by Grozema et al. [14] showed that I^- is likely to accept an electron from the donating phenyl group (from SAN) to form CTC; thus, the phenyl group acts as an electron-donor. In the case of I_2, however, the group serves as an electron-acceptor and becomes a site for CTC formation [14]. The introduction of SAN monomers to I_2 is shown in Fig. 3a, while Fig. 3b shows a schematic diagram of the formation of CTC structures from phenyl–I_2 interactions in SAN, where modification of the ion storage property occurs. Such modification further improves the conductivity of the ion.

Figure 3c and d illustrate the formation of iodide and the resulting formation of triiodide, respectively, based on Eq. 1. These results further confirm that SAN manages to host both I^-/I_3^- redox couples for continuous QSSC activity. The encapsulation of the I^-/I_3^- redox couple liquid electrolyte in SAN is possible with EC and PC as plasticizers-cum-solvents, leading to the formation of a SAN/NaI/I_2/EC/PC GPE for QSSCs.

Impedance characteristics

The disassociation of 0.5 M NaI and 0.05 M I_2 provided a constant amount of I^- and I_3^-, thus forming a "standard" liquid electrolyte. The continuous increment of bulk resistance could be observed when more I_2 (having a certain affinity to its phenyl group) diffuses into the SAN network with the addition of electro-inactive SAN. This was also observed by Trchova et al. [15] during the bonding of chlorine to the aromatic rings of polyaniline; in this work, a decrease in the bulk conductivity of the films was observed.

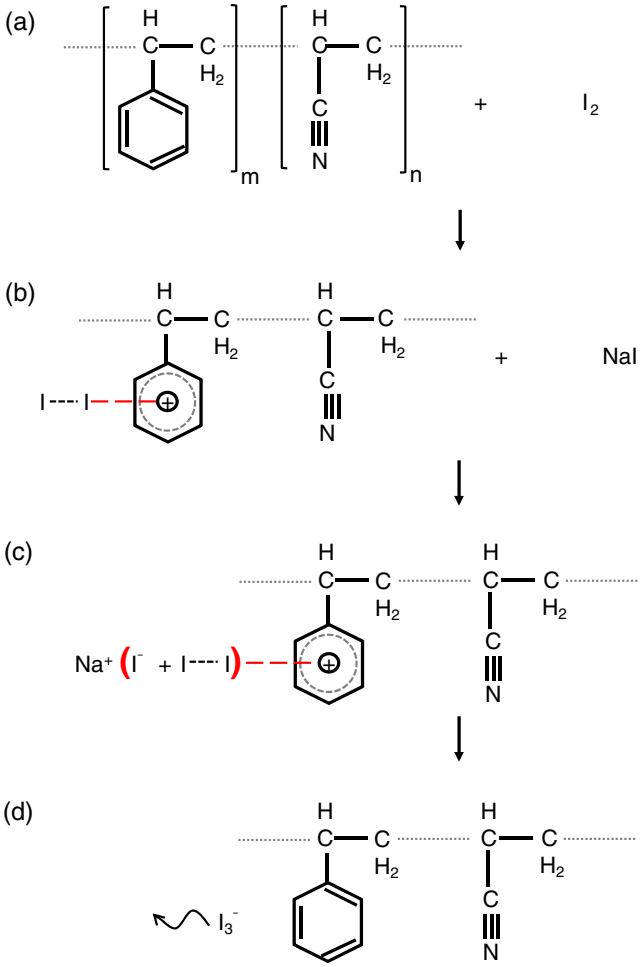

Fig. 3 Schematic diagram of SAN and I_2 CTC formation

Theoretically, the electrodes should exhibit ideal capacitive impedance in the absence of charge transfer processes [16]. However, because this system is not ideally capacitive, charge transfers exist in it. Defects on the stainless steel electrode, such as scratches and contamination, result in capacitive dispersion [17]. Over a wide range of frequencies, such effects can be described by the empirical concept of a constant phase element (CPE) [18]. This can be derived by Eq. 4 [16]

$$Z(\omega) = K(j\omega)^{-\alpha} \tag{4}$$

where K is the numerical value of admittance ($1/|Z|$) at ω= 1 rad s^{-1} and α has a value between 0.5 and 1 for an irregularly surfaced electrode [19]. The CPE behavior can be quantified by incorporating Eq. 4 into Fig. 4. By plotting the imaginary impedance (Z'') as a function of logarithmic frequency, the gradient of the plot becomes the α value. Note that $\omega=2\pi f$, where f denotes the frequency. Table 2 shows the varieties of the gradient values; the α values are in the 0.5−1.0 range. The varieties of the gradient values were caused by the inhomogeneous measuring electrode surface.

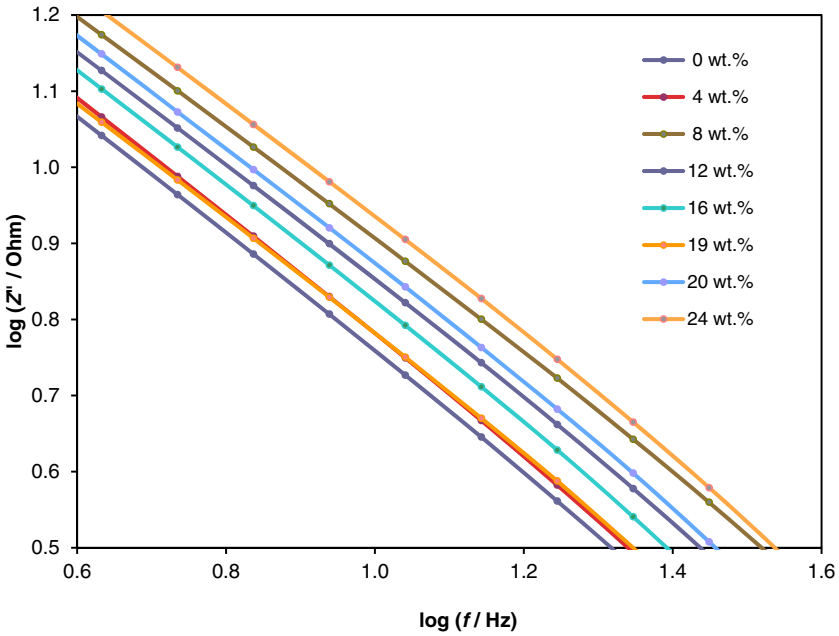

Fig. 4 Logarithmic imaginary impedance as a function of frequency of GPEs with different SAN concentrations

Shear stress versus strain rate plot

Figure 5 describes the shear stress (τ) and strain rate (γ) between polymer molecules in I^-/I_3^- solution, which depend strongly on the SAN content. Obviously, τ increases drastically with the constant increase of γ, and measures higher in terms of mechanical strength with increasing SAN content in the GPE. The trend of increasing slope that intercepts at the origin with higher SAN content indicates increasing viscosity (η). The viscosity of a polymer is an interesting subject that must be clearly understood to determine its role in the interaction of polymer chains, their structures, and entanglement [20]. Initially, a value of η equal to 0.041 Pa s is recorded at 0 wt.% SAN. This value drops slightly to 0.023 Pa s at 4 wt.% SAN, increases back to 0.096 Pa s at 8 wt.% SAN, and then continues to increase to 0.324, 0.887, 1.445, 1.903, and 4.186 Pa s at 12, 16, 19, 20, and 24 wt.% SAN, respectively.

Based on the linear relation between τ versus γ plot that passes through the origin (Eq. 5), SAN/NaI/I_2/EC/PC mixtures appear to exhibit Newtonian-like behavior. However, this phenomenon is rare for a polymeric material. Bonding between SAN and a "standard" liquid electrolyte is almost nil compared with the weak hydrogen bonding between water, as indicated by Newtonian behavior. The Newtonian-like behavior proves that a weak bond that mimics the hydrogen bonding was resulted in the formation of the CTC.

$$s = \eta\left(\frac{d\gamma}{dt}\right) \tag{5}$$

Figure 6 shows the trend of the diffusion coefficient D, which is inversely proportional to η and supported by Eq. 6, with increasing SAN content. D was calculated based on Eq. 6 [21]:

$$D = \frac{kT}{6\pi\eta r} \tag{6}$$

where k denotes the Boltzmann constant, T is the temperature in Kelvin, and r is the radius of sphere. In this calculation, the shapes of I^- and I_3^- are assumed to be spheres that have a constant radius of 2.11 [22] and 104 Å [2], respectively. It is clear that the D of I_3^- is considerably smaller than that of I^- due to movement restrictions brought about by its ionic size [23]. Figure 7 also shows D increments from 2.6×10^{-9} to 4.5×10^{-9} cm^2 s^{-1} for I^- and 5.2×10^{-11} to 21.9×10^{-11} cm^2 s^{-1} for I_3^- after 4 wt.% SAN was introduced to the electrolyte. Further additions appeared to impede ion migration. The instant D increment observed was due to the attractive forces between I_2 and the phenyl group; these forces increased the D values drastically.

Table 2 Gradient values of the logarithmic Z'' versus logarithmic frequency plot

SAN content (wt.%)	Gradient	α
0	−0.7712	0.7712
4	−0.7766	0.7766
8	−0.7311	0.7311
12	−0.7580	0.7580
16	−0.7594	0.7594
19	−0.7588	0.7588
20	−0.7670	0.7670
24	−0.7509	0.7509

Conductivity and viscosity characterization

Secondary evaluations of impedance and τ versus γ plots are based on the conductivity, σ, and η, as shown in Fig. 7. While

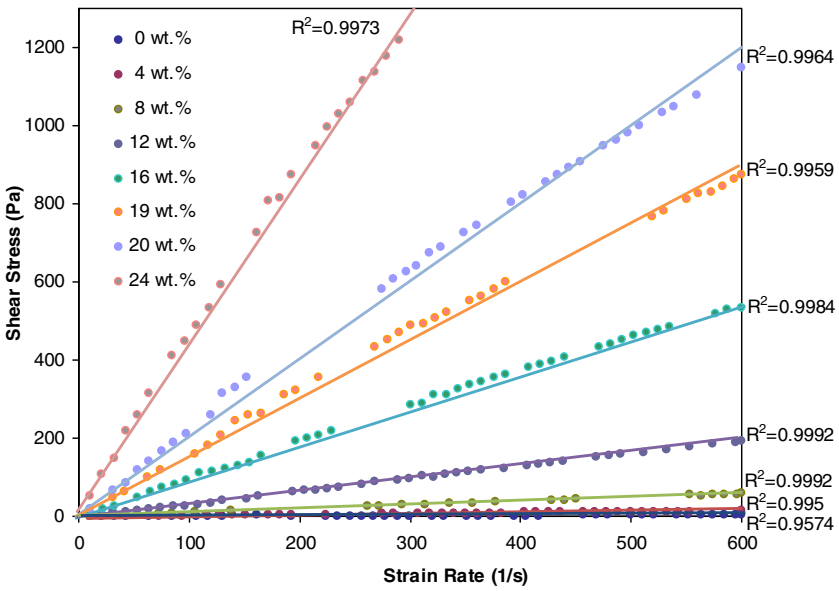

Fig. 5 Shear stress versus strain rate curves of GPEs with different SAN concentrations

η shows an increase in value, the σ shows a continuous linear decrease in value to 4.54, 3.83, 3.02, 2.55, 1.89, 1.49, 1.35, and 0.83 Scm^{-1} at 0, 4, 8, 12, 16, 19, 20, and 24 wt.% SAN. However, the average viscosity of the samples with >19 wt.% SAN increased drastically, as shown by the increase in gradient. The sudden increase observed suggests the initiation of gelled conditions in samples with 19 wt.% SAN and viscosity values above 1 Pa s. The compromised balance between optimized ionic conductivity from NaI/I_2 and viscosity was observed at 19 wt.% SAN. Both findings are similar to those by Deepa et al. [9] and Southall et al. [24]. Balance between conductivity and gelled properties could only be achieved in electrolytes with 19 wt.% SAN.

Three different scenarios were described for electrolytes with (*a*) <19, (*b*) =19, and (*c*) >19 wt.% SAN. Samples with <19 wt.% SAN indicated that NaI and I_2 were not ionically cross-linked to SAN when they obeyed Newton's law (Eq. 6). Newton's law describes the applied shear stress as proportional to the rate of strain $d\gamma/dt$ [25] shown by the linear plot in Fig. 5.

Electrolyte encapsulation by <19, =19, and >19 wt.% SAN

A schematic diagram of the arrangement of isolated SAN chains in elevated content gradient is shown in Fig. 8. These isolated chains were assumed to be spheres of coiled SAN. In general, the molecules were well separated in dilute solutions (low SAN contents) [26] and did not interact with each other (Fig. 8a). Therefore, the molecules can be imagined to be parts of an isolated chain. Relatively high σ values were recorded due to wider conducting pathways

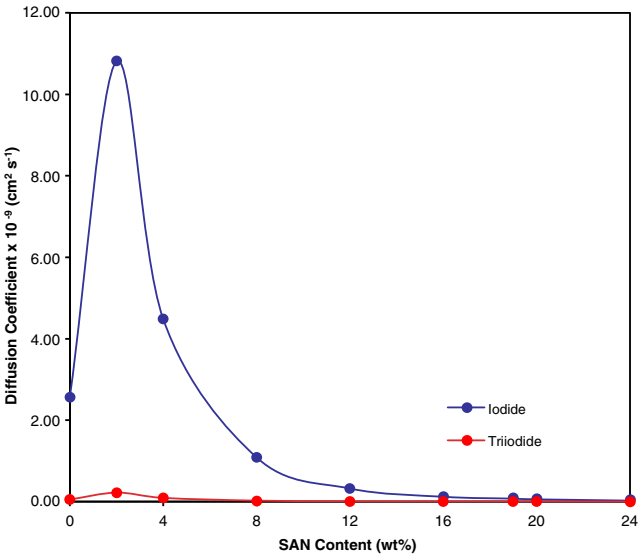

Fig. 6 Diffusion coefficients of GPEs with different SAN concentrations

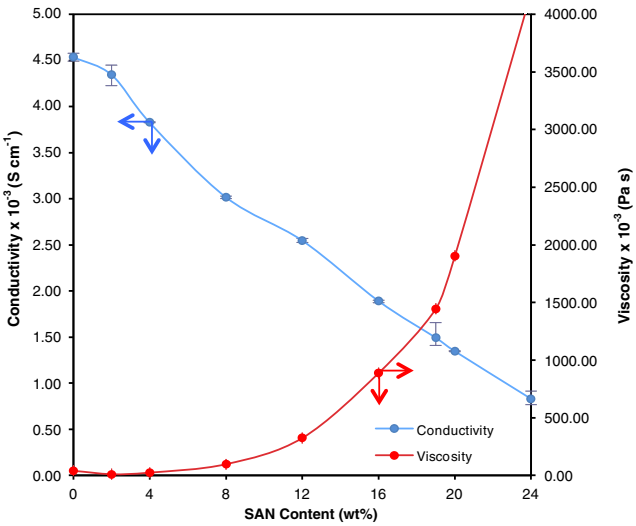

Fig. 7 Conductivity and viscosity relation of GPEs with different SAN concentrations

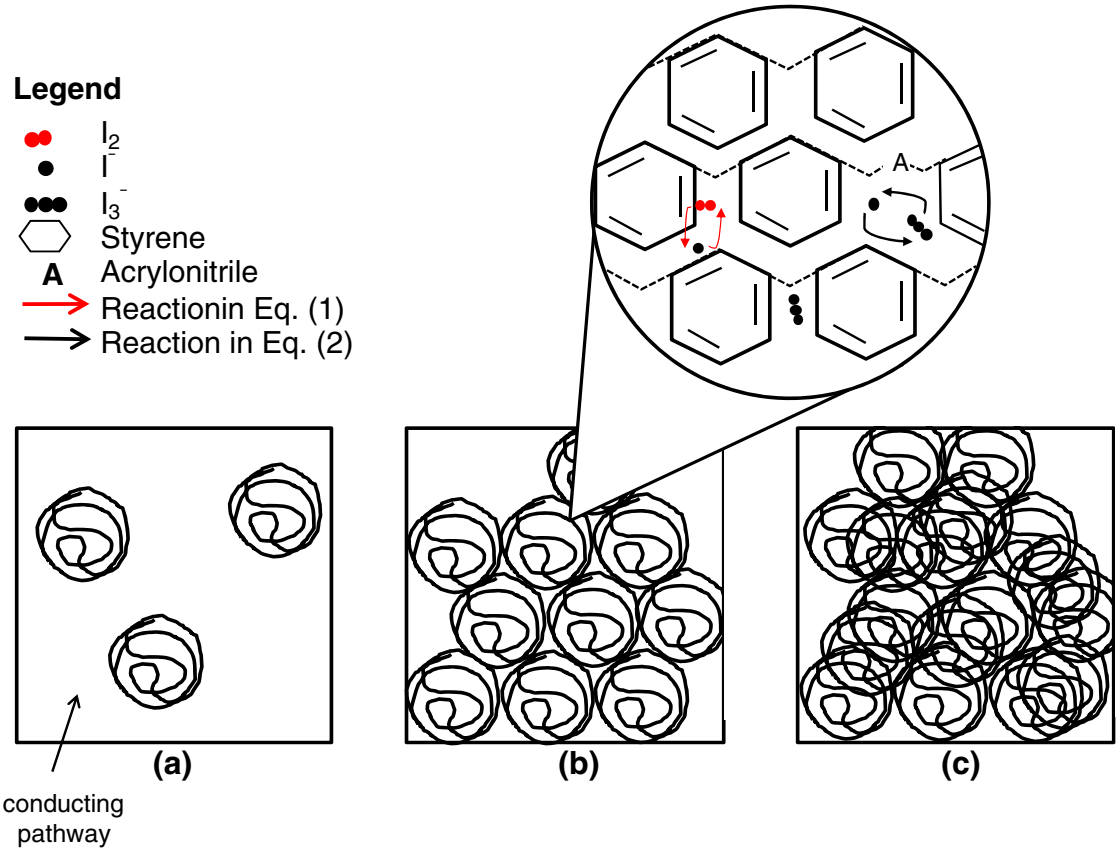

Fig. 8 Schematic diagram of SAN coils at **a** <19, **b** =19, and **c** >19 wt.% SAN

between the coils. The η suggests that coils of SAN and liquid electrolyte "flow" along their respective planes with minimal resistance created from the friction between coils. Low η values may also be due to the presence of coils of long chains, which, because they are not (or only slightly) anchored, continue to slide (chain slippage) during η measurement. This further suggests the inadequacy of the amount of SAN for mechanical support in the 0.5 M NaI and 0.05 M I_2 liquid redox electrolyte.

Figure 8b illustrates the optimum gelled condition. In this condition, contact between coils at 19 wt.% SAN was sufficient to provide an adequate number conducting pathways in a mechanically stable form. A magnified schematic diagram shows the proposed mixed reactions that could occur in the conducting pathways between straightened main chain coils of SAN in a QSSC application. The I_2 tends to be held by weak CTC bonds within the phenyl group [2, 27], forcing its main chains into a spatial arrangement. This was proven by the ring torsion detected during the FTIR spectra measurement.

In this case, the rate with which I^- (2.11 Å) diffuses into the SAN network is significantly higher than that with which I_3^- (104 Å) diffuses out. I_3^- diffusion through a gel may proceed slowly because of the large size of the molecule. Adequate chain relaxation in SAN is required for the ion to move to a new location (i.e., the counter electrode) to promote continuous redox interaction in a QSSC application. A similar study by Saito et al. [23] supported the observation that fast diffusion processes can be attributed to the inability of the liquid electrolyte (mainly I^-) trapped in the network to disperse into the polymer. Thus, addition of 19 wt.% SAN ensures sufficient formation of conducting pathways on the outer side of the spherical SAN coils (mimicking the capillary wetting of water).

The use of excess concentrations of SAN, >19 wt.% SAN, for encapsulating liquid redox electrolytes resulted in the lowest σ. In Fig. 8c, coils that overlap narrowed the conducting pathways between chains and prevented the formation of the CTC. Restrictions during sheared deformation between the coiled main chains of SAN in this electrolyte mixture were basically nil, while the friction between the chains was considerably higher than in mixtures with lower SAN contents. The higher friction observed was due to the increased presence of rigid structures, such as large phenyl groups, overlapping with each other along several flow planes resulting in an elevated "viscous drag" with increasing SAN concentrations [25].

The electrolyte with >19 wt.% SAN is also prone to tangling between long chains, proven by bond torsion exhibited in the FTIR result (Fig. 2). It should be noted that

the η values of the 24 wt.% SAN sample were only readable at a strain rate of ≤300 s^{-1}. This may have been caused by the limited extension capacity during shear testing, which may be related to the maximum straightening [20] of the overlapping chains. In other words, samples containing >19 wt.% SAN were too rigid for the application.

Conductivity—thermal dependence behavior

Samples ranging from 0 to 24 wt.% SAN were thermally tested up to 100 °C. In Fig. 9, the logarithmic σ shows the average increment of all samples with or without SAN with increasing temperature. Temperature plays an important role in increasing D [28], and, consequently, the bulk σ. Decreasing σ values in the Arrhenius plot were also observed with increasing SAN content in the electrolyte mixture. The liquid electrolyte without SAN shows a relatively linear curve with increasing temperature in comparison with the obvious curve obtained upon the addition of SAN. The curve became more apparent increasing concentrations of SAN up to 24 wt.%; this suggests a non-Arrhenius-like temperature-dependent behavior [29]. Pas et al. [30] claimed that the hallmark of non-Arrhenius-like behavior is the decoupling of ionic motions with the host matrix. The results prove that ionic motion occurred when CTC-bound I_2 was decoupled [30] from the phenyl group in SAN to form I_3^-.

Potential stability and applicability of 19 wt.% styrene–acrylonitrile in QSSC

Researchers have shown that the potential use of QSSCs was limited to only 1.0 V [31, 32]. Others have demonstrated their lowest use at −1.0 V [33]. To measure the applicability of the gel electrolyte in a QSSC, LSV measurements were carried out; these resulted to a stability window (Fig. 10) for the highest-conducting electrolyte (19 wt.% SAN) ranging from −1.68 to 1.38 V. This shows that the stability of the SAN-based electrolyte does not exceed the normal potential range from −1.0 to 1.0 V, and indicates that it is suitable for QSSC applications. To test electrolyte applicability, a SAN/NaI/I_2electrolyte was assembled along with a ZnO photoanode and an ITO photocathode. The functionality of the resulting setup is shown in Fig. 11.

A liquid electrolyte was embedded into the graph as a control sample for comparison with the SAN-based electrolyte. Although the liquid electrolyte showed higher potentials than the SAN-based one, the former maintained its diode-like characteristics. The electrolyte showed intercepts at both the X- and Y-axes of the I–V curve (Fig. 11). Short circuit current (I_{sc}) values of 0.55, 0.41, 0.08, and 0.03 mA were obtained from samples of liquid-based and gelled electrolytes under alternating illuminated and dark conditions. Plots from both illuminated and dark conditions showed similar open-circuit

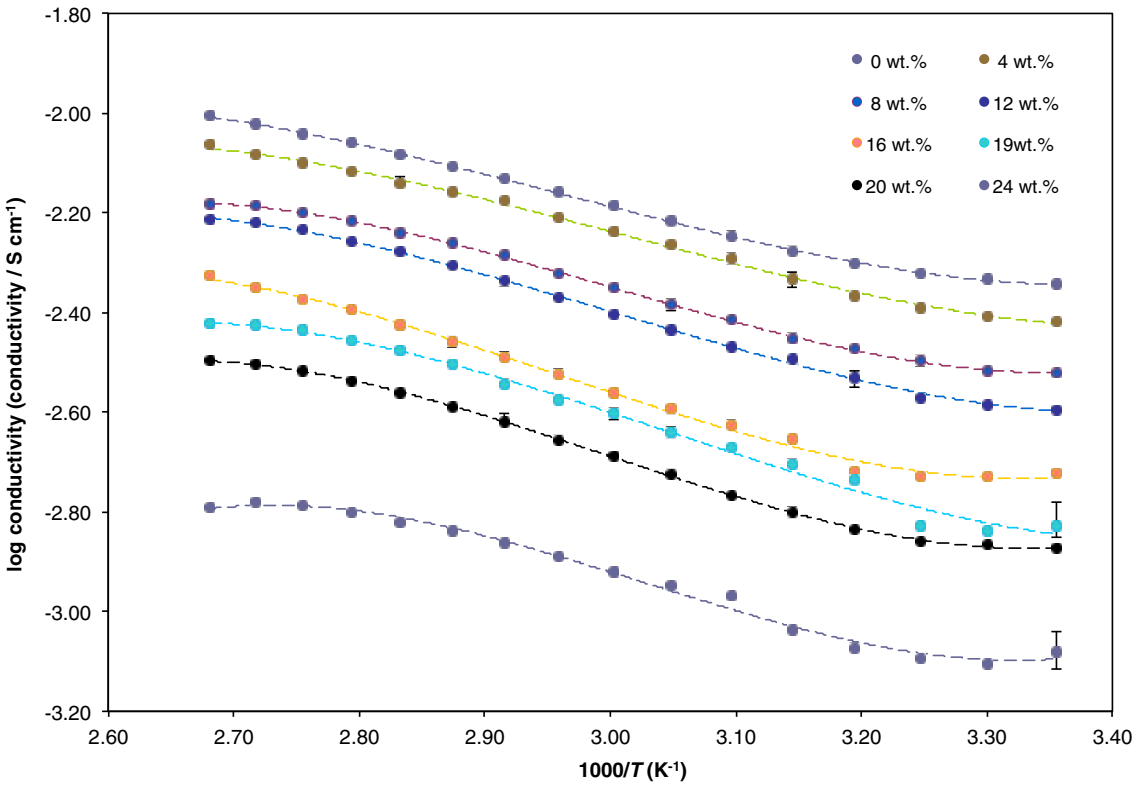

Fig. 9 Conductivity temperature-dependence plots of GPEs with different SAN concentrations

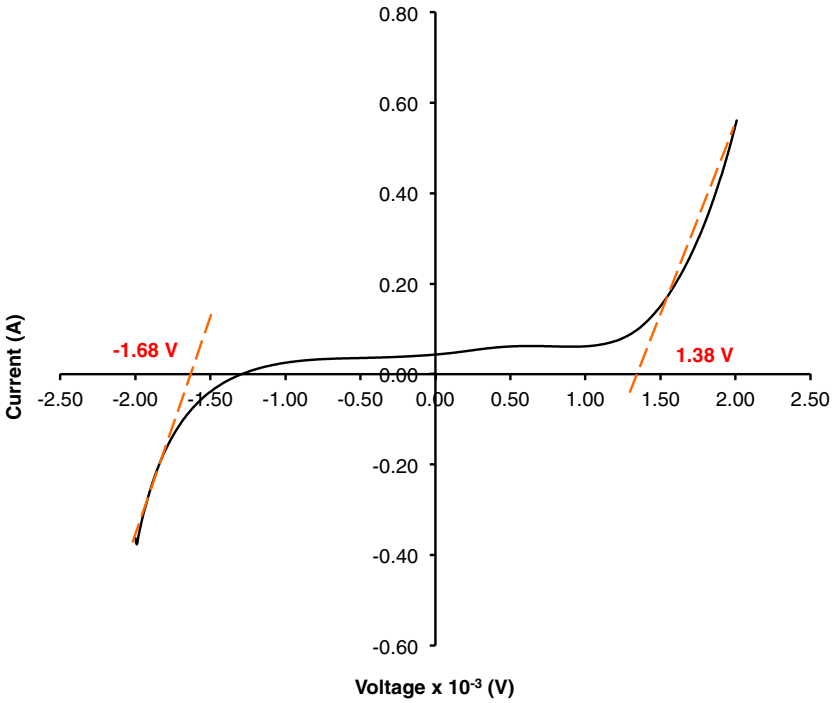

Fig. 10 LSV curve of the GPE containing 19 wt.% SAN

voltage (V_{oc}) readings at 0.45 V (liquid electrolyte) and 0.34 V (SAN-based electrolyte).

In comparison with both liquid and gelled electrolytes, SAN-based electrolytes showed a smaller *I–V* plot. This is mainly due to the lower conductivity of the electrolyte with 19 wt.% SAN. On the other hand, liquid-based electrolytes yielded difficulties in placement between both photoanodes during QSSC measurements since it showed a tendency to leak, as evidenced by its short circuit *I–V* trend. Thus, the utilization of 19 wt.% SAN was maintained during practical *I–V* measurements.

Conclusion

The addition of SAN into NaI/I_2 liquid electrolytes does not affect the structural bonding of the liquid electrolyte. However, SAN introduction causes ring torsion. During encapsulation of a liquid redox electrolyte, the coiled chains of SAN tend to distort, allowing I_2 and I^- to seep in and form a GPE. The decline in σ and a rare Newtonian flow in the GPE are observed, suggesting that both the electrolyte and SAN are not ionically cross-linked. The production of independent coiled up main chains surrounded by conducting

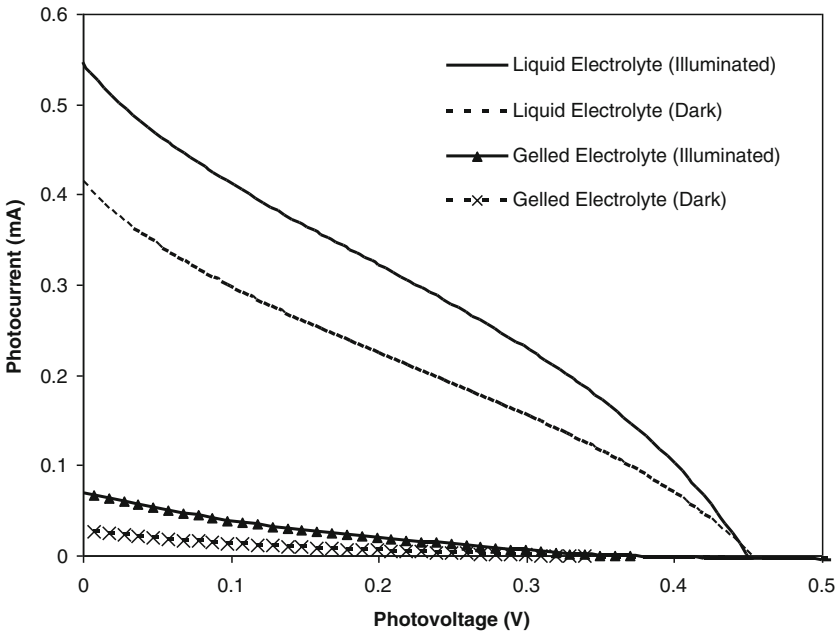

Fig. 11 *I–V* characteristics of the assembled QSSC using the GPE with 19 wt.% SAN

pathways is thus proposed. At higher SAN contents, overlapping of the coils occurs; these minimize conducting pathways, as shown by the lowered conductivity values obtained. The tendency of phenyl structures to hook to each other is demonstrated. Consequently, higher ring torsion, as determined via the FTIR spectra, and maximum extension capacity, as determined via the shear stress tests, are observed. Both electrical and mechanical properties are optimized at 19 wt.% SAN, as observed via the σ and η values, respectively. SAN also shows non-Arrhenius-like behaviors with elevated temperatures and electrical stability within the range of −1.68 up to 1.38 V. Photocurrents induced by the *I*–*V* plot support the usability of SAN for encapsulating NaI and I_2 liquid electrolytes.

Acknowledgment The authors would like to thank the Short Term Grant 6039030, USM-RU-PRGS 8031030, MOSTI for the National Science Fellowship award and the USM Fellowship P-GM 0331 for their financial support.

References

1. Saikia D, Han CC, Chen-Yang YW (2008) J Power Sources 185:570–576
2. Ramani R, Ramachandra P, Ramgopal G, Ranganathaiah C (1998) J Appl Polym Sci 68:2077–2085
3. Ileperuma OA, Dissanayake MAKL, Somasunderam S, Bandara LRAK (2004) Sol Energy Mater Sol Cells 84:117–124
4. Panwar V, Kang B, Park J-O, Park S, Mehra RM (2009) Eur Polym J 45:1777–1784
5. Silva ALA, Takase I, Pereira RP, Rocco AM (2008) Eur Polym J 44:1462–1474
6. Lan Z, Wu J, Wang D, Hao S, Lin J, Huang Y (2006) Sol. Energy 80:1483–1488
7. Dissanayake MAKL, Bandara LRAK, Bokalawala RSP, Jayathilaka PARD, Ileperuma OA, Somasundaram S (2002) Mater Res Bull 37:867–874
8. Sekhon SS (2003) Bull Mat Sci 26:321–328
9. Deepa M, Sharma N, Agnihotry SA, Singh S, Lal T, Chandra R (2002) Solid State Ionics 152–153:253–258
10. Yap CK, Tan WC, Alias SS, Mohamad AA (2009) J Alloy Compd 484:934–938
11. Tan WC, Mohamad AA (2010) J Electrochem Soc 157:E184–E190
12. Chowdhury A, Thynell ST (2007) Thermochim Acta 466:1–12
13. Dyson RW (1998) Specialty Polymers 2nd ed. Blackie Academic & Professional, United Kingdom, P9
14. Grozema FC, Zijlstra RWJ, Swart M, Duijnen PTV (1999) Int J Quantum Chem 75:709–723
15. Trchová M, Sedenková I, Tobolková E, Stejskal J (2004) Polym Degrad Stabil 86:179–185
16. Pajkossy T (2005) Solid State Ionics 176:1997–2003
17. Ricciardi S, Ruiz-Morales JC, Nuñez P (2009) Solid State Ionics 180:1083–1090
18. Chen W, Tang H, Ou Z, Wang H, Yang Y (2007) Electrochim Acta 53:2065–2070
19. Rammelt U, Reinhard G (1990) Electrochim Acta 35:1045–1049
20. Haward RN, Young RJ (1997) The physics of glassy polymers. Chapman & Hall, United Kingdom, p 18
21. Wang Y, Sun Y, Song B, Xi J (2008) Sol Energy Mater Sol Cells 92:660–666
22. Yildiran H, Ayata S, Tuncgenc M (2007) Ionics 13:83–86
23. Saito Y, Stephan AM, Kataoka H (2003) Solid State Ionics 160:149–153
24. Southall JP, Hubbard HVSA, Johnston SF, Rogers V, Davies GR, McIntyre JE, Ward IM (1996) Solid State Ionics 85:51–60
25. Carraher CEJ (2008) Polymer Chemistry, 7th edn. Taylor & Francis Group, USA, p 229
26. Hamley IW (2000) Introduction to soft matter; polymers, colliods, amphiphiles and liquid crystal. Wiley, England, p 76
27. Svorcík V, Prosková K, Hnatowicz V, Rybka V (1999) Nucl Instrum Methods Phys Res Sect B-Beam Interact Mater Atoms 149:312–318
28. Buchholz FL, Graham AT (1998) The structure and properties of superabsorbent polyacrylates. In: Buchholz FL (ed) Modern superabsorbent polymer technology. Wiley, USA, p 199
29. Taggougui M, Diaw M, Carré B, Willmann P, Lemordant D (2008) Electrochim Acta 53:5496–5502
30. Pas SJ, Ingram MD, Funke K, Hill AJ (2005) Electrochim Acta 50:3955–3962
31. Yum J-H, Humphry-Baker R, Zakeeruddin SM, Nazeeruddin MK, Grätzel M (2010) Nano Today 5:91–98
32. Guillén E, Fernández-Lorenzo C, Alcántara R, Martín-Calleja J, Anta JA (2009) Sol Energy Mater Sol Cells 93:1846–1852
33. Stergiopoulos T, Arabatzis IM, Cachet H, Falaras P (2003) J Photochem Photobiol A-Chem 155:163–170
34. Ikezawa Y, Ariga T (2007) Electrochim Acta 52:2710–2715
35. Ikezawa Y, Nishi H (2008) Electrochim Acta 53:3663–3669
36. Maillo J, Pages P, Vallejo E, Lacorte T, Gacen J (2005) Eur Polym J 41:753–759